ELSEVIER

Thin Solid Films 414 (2002) 296–303

thin solid films

www.elsevier.com/locate/tsf

Breakdown of ultrathin anodic valve metal oxide films in metal-insulator-metal-contacts compared with metal-insulator-electrolyte contacts

Achim W. Hassel[a,*], Detlef Diesing[b]

[a]*Max-Planck-Institut für Eisenforschung GmbH, Max-Planck-Str. 1, 40237 Düsseldorf, Germany*
[b]*Institut für Physik der kondensierten Materie, Heinrich-Heine-Universität Düsseldorf, Universitätsstr. 1, 40225 Düsseldorf, Germany*

Received 10 April 2001; received in revised form 30 November 2001; accepted 23 January 2002

Abstract

The anodic breakdown of thin valve metal oxide films on aluminium, hafnium, niobium, titanium, tantalum and zirconium in the system valve-metal/valve-metal-oxide/silver was investigated. For all systems valve metal wires covered by an anodically formed oxide with an evaporated silver film were used. For comparison three different types of oxide were used in the case of aluminium: anodic oxide, gas phase oxide and physical vapour deposited oxide. Due to an improved technique for the preparation a high reproducibility and reliability could be achieved. In the case of anodic oxide it is shown, that the formation field strength or reciprocal film formation factor and the breakdown field strength are equal. The initial step of anodic breakdown is clearly an ionic one. This was concluded from the strong correlation between film thickness and breakdown potential. An equation for the absolute quantitative calculation of tunnel currents is derived that takes the deformation of the barrier due to the image potential into account. The simulations are compared with the experimental results and the breakdown process is discussed in terms of ions which move into the tunnel barrier and deform the tunnel barrier.

Keywords: Electrochemistry; Anodic oxidation; Tunnelling; Aluminium oxide; Aluminium; Hafnium; Niobium; Tantalum; Titanium; Zirconium; Breakdown

1. Introduction

Valve metal oxides are almost perfect insulators. Those dielectric films are used in capacitors [1], in tunnel junctions [2] and for insulation of semiconductors [3]. One of the basic requirements is the ability to withstand an electric field of 0.1–1 GVm^{-1} without electric breakdown. Due to the enormous industrial importance there is a tremendous number of investigations dealing with the breakdown of these films. A number of reviews by Agarwal [4], Solomon [5], Klein [6], DiStefano and Schatzkes [7], Ikonopisov [8] and the one by Parkhutik, Albella and Martinez-Duart [9] lead to an overview over this wide field. The stability of the film and the mechanism of the breakdown process depend on the base metal, its purity and structure, on the process of oxide formation, the oxide thickness and the type and composition of the adjoining phase. There are a lot of investigations of the breakdown of anodic valve metal oxide films in the electrolyte or in a metal-oxide-metal contact. However, there are very few on the breakdown of thin (1–20 nm) barrier type anodic valve metal oxide films.

This work focuses on the breakdown of tunnel junctions of the type valve metal (Al, Hf, Nb, Ta, Ti and Zr)/anodic valve metal oxide/silver. From the previous work it is known that the oxidation process is a key parameter for the properties and stability of these layer systems. Thereby a short introduction into the anodic oxidation process is given.

2. Theoretical

The oxidation of valve metals can be described by the high field law of oxide formation

$$i = i_0 e^{\beta E} \quad (1)$$

*Corresponding author. Tel.: +49-211-6792-464; fax: +49-211-6792-218.
E-mail address: hassel@elchem.de (A.W. Hassel).

0040-6090/02/$ - see front matter
PII: S0040-6090(02)00453-4

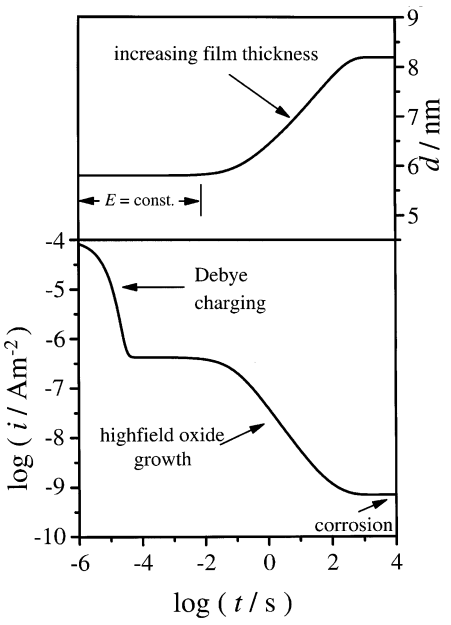

Fig. 1. Current transient calculated from the classical high field law of oxide growth, taking into account the Debye charging of the oxide and the corrosion current (lower) and transient of the film thickness calculated through integration of the current transient (upper).

This equation describes the relation between the oxide formation current i, the initial current density i_0, the high field constant β and the field strength E. This is given by

$$E = \frac{\Delta U}{d} \tag{2}$$

where ΔU is the potential drop over the insulating film and d is its thickness. In the lower part of Fig. 1 calculated current transient of additional oxide formation on an aluminium/aluminium oxide specimen with a 5.8 nm thick initial oxide film is shown. This oxide film was formed in a pH 6.0 acetate buffer by potentiotstatic polarisation to $E_{\mathrm{HESS}} = 2$ V (HESS = hydrogen evolution in same solution). The transient was recorded after a potential step from $E_{\mathrm{HESS}} = 0$ V to $E_{\mathrm{HESS}} = 3.5$ V. The Debye charging (Charging of the oxide capacitance in the metal/insulator/electrolyte system) of the oxide as well as the corrosion current are taken into consideration. In the upper part of the figure the corresponding thickness transient is shown as a function of time as calculated through the numerical integration of the current transient.

This change in thickness Δd was calculated from Eq. (3).

$$\Delta d = \frac{qM_V}{zF\rho_{ox}} \tag{3}$$

Where q is the charge density, M_v is the volume of 1 mol oxide, z is the number of transferred electrons, F is the Faraday constant and ρ_{ox} is the density of the oxide.

The experimental current transients of high time resolution were already shown in a former paper [10]. They show several additional processes such as dielectric relaxation and a kinetic transport hindrance resulting in an overshooting current during oxide formation. Since these processes were discussed there they are not especially relevant for the following discussion: they are skipped here. Here it seems to be more appropriate to discuss the process of oxide formation on hand of the simplified theoretical calculation instead of the much more complicated experimental curves.

Within the first few μs after a potential step the current density in Fig. 1b decreases from A cm^{-2} down to a few mA cm^{-2}. This sudden decrease is due to the Debye charging of the oxide capacity over the electrolyte resistance. It is seen in Fig. 1b that the current becomes constant after the charging of the oxide film for 10^{-4} s $< t < 10^{-2}$ s. In the first decades of time the charge, calculated from the integration of the current, is very small. Hence, the oxide thickness remains almost constant. Later the charge accumulates to a significant amount as can be seen in the thickness transient after 10^{-2} s. Due to the increasing oxide thickness the field-strength decreases accordingly in this potentiostatic experiment. With this decreasing fieldstrength the driving force of further oxide formation decreases. This can be seen in the lower part of the figure as the current decreases with time. Finally, when the current density is in the order of the corrosion current density, the film thickness becomes constant.

Under these stationary conditions a small amount of oxide is dissolved in a given time unit. At the same time new oxide is formed. Since oxide reformation and corrosion are equal but with different sign, the corrosion current can be measured directly. Due to the constant current and constant film thickness under these conditions the product of charge carrier concentration and charge carrier mobility must be constant. It was already explained that under these conditions, where oxide is formed on both interfaces but corrosion takes place only at the oxide/electrolyte interface the oxide layer moves into the metal. During this process the whole oxide is converted into a pure anodic oxide independent on how its structure was before. Also initial gas phase oxide coverages are removed by this technique. It is essential for understanding the following results that under these conditions the potential drop across the oxide film and the oxide film thickness are constant and hence, also the fieldstrength.

By a comparison of **m**etal/**i**nsulator (metal oxide)/**e**lectrolyte systems (MIE) and **m**etal/**i**nsulator (metal oxide)/**m**etal systems (MIM) it is shown that the breakdown in the MIM systems appears exactly and

highly predictable at fieldstrengths, where further oxide growth would start in the corresponding MIE system. A preparation technique is described which allows a reproducible production of that MIM specimens. Various preparation parameters will be discussed in terms of their influence on the stability of the tunnel junctions. A breakdown mechanism similar to that of Shousha [11] is described, which was derived from the model of high field oxide growth as proposed by Lohrengel [12].

It is important to say that the breakdown stability depends not only on the oxide thickness but very much on the formation conditions. If the oxide is formed in shorter times, e.g. 100 s the film thickness would be 7.8 nm instead of 8.2 nm in Fig. 1. This decrease in oxide thickness of approximately 5% results in a 40% decrease of the breakdown voltage. In addition the reproducibility is much worse. Hence, a basic knowledge of the transient behaviour during oxide formation is essential to understand the strong influence of the oxide formation conditions on the properties of metal-insulator-metal contacts.

The present work is focused on the tunnelling process and the comparison with metal/insulator/electrolyte systems.

3. Experimental

All sample wires were provided by Goodfellow. The solutions were prepared from reagent grade chemicals and high purity water Millipore Q ($R_s > 18$ MΩ cm).

Electropolishing was carried out either in a mixture of 50 ml 70% perchloric acid and 950 ml glacial acetic acid (Al, Hf, Ti) or in a mixture prepared from 10 ml 40% hydrofluoric acid and 90 ml 96% sulphuric acid (Nb, Ta, Zr). The oxide films were formed in 1 kmol m^{-3} sulphuric acid (Hf, Ti, Zr) or in a neutral acetate buffer (pH = 6.0) (Al, Ta, Nb), prepared from water, glacial acetic acid and sodium acetate with an ionic strength of 10^6 mol^2 m^{-6} (1 mol^2 l^{-2}). All experiments were carried out in dry nitrogen at $T = 298$ K (Table 1).

The UHV Chamber was a Riber System with a turbo molecular pump, an ion getter and a kryo pump. The base pressure was $1 \cdot 10^{-6}$ Pa. During evaporation of aluminium or silver the pressure was held at $1 \cdot 10^{-5}$ Pa. The thickness of the evaporated films was determined with a VEECO quartz crystal micro balance. During the evaporation of silver top electrode the wires were rotated in a distance of 30 cm from the evaporation source to minimise thermal stress and to ensure a homogeneous silver thickness on the wires.

Furthermore, details of the experimental set-up and the procedure for preparing the tunnel junctions were described in a previous paper [10].

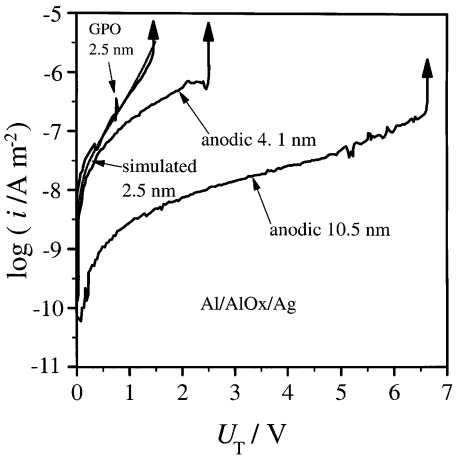

Fig. 2. Tunnel characteristics of different aluminium/aluminium oxide/silver contacts at $T = 298$ K. The experimental curves were recorded with a sweep rate of 100 mV s^{-1}. For the GPO system a 2.5 nm thick oxide was taken. The anodic oxide films were formed at a formation voltage of $E = 1$ V ($d_1 = 4.1$ nm) or $E_{HESS} = 5$ V ($d_2 = 10.5$ nm). The breakdown potential of each contact is indicated by an arrow. Calculated tunnel curves are given for comparison. Details of the calculation procedure and the basic barrier properties are given in the text.

4. Results

Fig. 2 shows current voltage plots of three different anodic aluminium/aluminium oxide/silver tunnel junctions. For the GPO system a 2.5 nm thick oxide was taken. The anodic oxide films were formed at a formation voltage of $E = 1$ V ($d_1 = 4.1$ nm) or $E_{HESS} = 5$ V ($d_2 = 10.5$ nm). The scan rate was 100 mV s^{-1}. Due to the high dynamic the current was plotted on a logarithmic scale. At low voltages the current is very small but increases rapidly as the potential increases. At voltages

Table 1
Electropolishing conditions for the different valve metals used in this study

Metal	Purity	Electropolishing solution	Time /s	Current density/ kAm^{-2}
Al	99.95%	$HClO_4/CH_3OOH$	30	2.00
Hf	97% (2.8% Zr)	$HClO_4/CH_3OOH$	10	1.20
Nb	99.9%	HF/H_2SO_4	20	1.00
Ta	99.95%	HF/H_2SO_4	300	1.00
Ti	99.975%	$HClO_4/CH_3OOH$	120	2.50
Zr	98.7% (1.1% HF)	HF/H_2SO_4	20	5.00

$|U| > 0.5$ V it gives a more or less straight line in the log i vs. U plot. If the potential exceeds a critical value E_{BD} a sudden increase is observed, which is indicated by the thick arrows at the end of each curve. This is the breakdown potential of the tunnel junction. As expected with increasing oxide thickness the current decreases and the breakdown potential increases.

The measured tunnel currents can also be derived theoretically. Duke performed model calculations for absolute values of tunnel current densities (in A/m^2) [13].

The equation used was:

$$i = \frac{e(2s+1)}{\hbar}\int_0^\infty (f(\mu) - f(\mu + eU_T))d\mu \int_0^\infty \frac{d^2k_{\|}}{2\pi^2}T(\mu) \quad (4)$$

where e is the elementary charge, s is the spin of the electron, $\hbar$ is the Planck constant, μ is the electron energy, $f(\mu)$ is the Fermi distribution in the two metals and $k_{\|}$ is the plane parallel momentum coordinate. In the equation above $T(\mu)$ is the decay factor of the Bloch wave of the metal electron in the oxide film. It can be derived by the Schrödinger equation:

$$-\frac{\hbar^2}{2m}\ddot{\psi} + V(z)\psi = \mu\psi \quad (5)$$

with the mass of the free electron m and the shape of the tunnel barrier $V(z)$. The decay factor of the Bloch wave of the electron as function of the z-coordinate axis (normal to the layer interfaces) is:

$$\kappa(z) = \sqrt{\frac{2m}{\hbar^2}} \cdot \sqrt{V(z) - \mu} \quad (6)$$

One has to take the integral over the whole oxide barrier:

$$K = \int_{z_1}^{z_2} \kappa(z)dz \quad (7)$$

Its exponential form gives the transmission factor $T(\mu)$.

$$T(\mu) = e^{-2K} = e^{-2\int_{z_1}^{z_2} \sqrt{\frac{2m}{h^2}} \sqrt{V(z) - \mu}\ dz} \quad (8)$$

In Eq. (7) the starting point z_1 and the final point z_2 of the integration are influenced by the image potential effects, which the tunnelling electrons cause in both the aluminium and the silver electrode. A formula for the image potential was given by Simmons [14].

The potential V_i of the electron with respect to the vacuum level, when it is at a distance of z from the metal surface is:

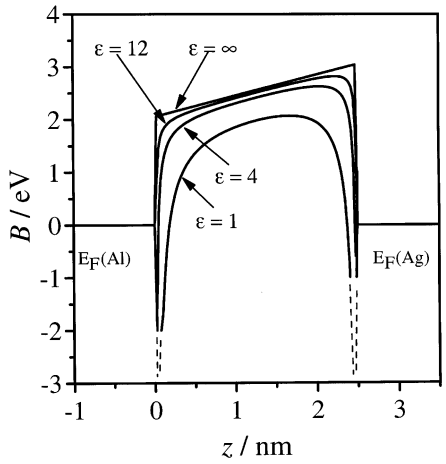

Fig. 3. Quantitative sketch of the asymmetric trapezoidal tunnel barrier in the MIM system A1/A1Ox/Ag with image potential corrections (for different dielectric constants) on which the calculated curve in Fig. 2 is based.

$$V_i = -\frac{1}{4 \cdot \pi \varepsilon_0} \cdot \frac{e^2}{4z} \quad (9)$$

In a MIM junction an electron exists between two parallel and closely spaced electrodes. The tunnelling electron polarises both of the electrodes. As a result both of the electrodes also influence the tunnelling electron. The image potential V_{image}, in this case can be derived by the following equation, where d denotes the thickness of the oxide layer:

$$V_{image}(z) = -\frac{e^2}{8\pi \cdot \varepsilon_0 \varepsilon_r} \cdot \left(\frac{1}{2z} + \sum_{n=1}^{\infty} \left(\frac{n \cdot d}{(n \cdot d^2) - z^2 - \frac{1}{n \cdot d}} \right) \right) \quad (10)$$

An approximation for the above summation term was given by Simmons [15].

When we set the origin of the z-coordinate axis at the geometrical metal/metal oxide interface using Simmons approximation for the sum in Eq. (10) the image potential corrections for an oxide layer with thickness d are given by:

$$V_{image}(z) = 0.795 \cdot \frac{-(e \cdot d)}{16 \cdot \pi \varepsilon_r \cdot \varepsilon_0 \cdot z \cdot (d - z)} \quad (11)$$

In Fig. 3 the asymmetric trapezoidal tunnel barrier for a 2.5 nm thick aluminium/aluminium oxide/silver MIM system is shown ($\varepsilon = \infty$). The difference between the Fermi Levels of the metals and the lower edge of the conduction band in the oxide were determined by the onset of the Fowler–Nordheim-tunneling to 2.05 eV on the aluminium/aluminium oxide interface and 2.71 at the aluminium oxide/silver interface [16,17]. This

tunnel barrier would be true only for a material with $\varepsilon_r = \infty$. Experimentally the ε_r, was found to be 4.5 in the case of PVD (physical vapour deposited) and 12 for anodic oxide [10].

The calculations of the barrier with image potential correction were carried out for a 2.5 nm thick aluminium oxide tunnel junction. The results of these calculations as well as the limiting case for vacuum ($\varepsilon_r = 1$) as insulator are shown in Fig. 3. The distortion of the conduction band of the oxide due to the image potential causes a shift of the real start of the tunnelling path of a few 100 pm as can be seen in Fig. 3. This shift is generally taken into account in our calculations of the current voltage plots (Eq. (4) and Eq. (7)). Additionally the current contribution due to the charging of the MIM capacitance at the experimentally used scan rate was taken into account.

In Fig. 2 the experimental results are compared with a calculated curve for $d = 2.5$ mn. They coincide quite well. This shows that the barrier type model for the direct elastic tunnelling process is adequate for this oxide thickness. If the same calculations are performed for the thicker anodic oxides, significant deviations from the experimental curves appear, therefore they are not shown here, Generally the calculated currents are smaller than the experimentally observed ones. The permittivity on the other hand does not change with increasing oxide thickness. This means that a simple barrier model for direct tunnelling is not valid for these samples. In fact a second contribution to the tunnel current for example by resonant tunnelling through defect states or diffusive tunnelling transport [18] can not be excluded. However, the share of the indirect tunnelling process is negligible in the case of the 2.5 nm thick oxide.

For a constant defect concentration the total amount of defects is proportional to the film thickness. Since these defects build the path for resonance tunnelling, the influence of the increasing film thickness is much less pronounced as in the case of the direct elastic tunnelling. In that case the well known exponential decay is valid. As a result the share of both tunnelling processes changes significantly with increasing film thickness. Haque and Khondker [18] used a statistical quantum mechanical ansatz to investigate the influence of defect states on the tunnelling transport of electrons. They found a transition from ballistic to diffusive transport regime with increasing number of defect states. A concrete evaluation of the tunnel path in anodic aluminium oxide and its experimental elucidation will be presented later since the extent of this paper would be exceeded.

In Fig. 4 the breakdown potential U_{BD} at $T = 298$ K for anodic polarisation of various MIM systems (aluminium/aluminium oxide/silver) is given as a function of the film thickness d. In the potentiostatic film formation procedure used here, the thickness corresponds

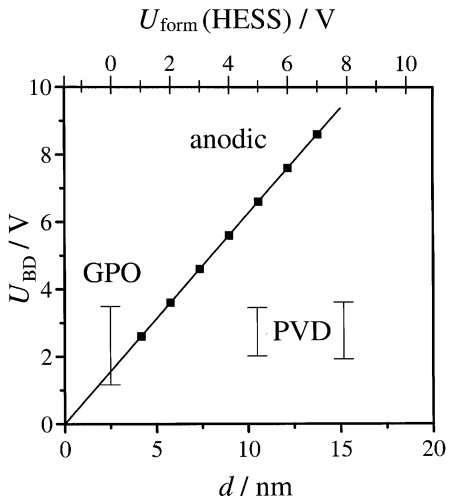

Fig. 4. Breakdown potential U_{BD} at $T = 298$ K for the anodic polarisation of various MIM systems (A1/A1Ox/Ag) as a function of the film thickness d. The formation potential for anodically formed oxides is given in the upper abscissa for comparison. GPO = gas phase oxide, PVD = physical vapour deposited oxide.

directly and linearly to the film formation potential U_{form}. [12]. This formation potential is given on the upper x-axis. The breakdown voltage vs. film thickness relation is described by an almost perfect line in the case of the anodic oxide films. This strong relationship between film formation potential and breakdown potential indicates a common origin. Furthermore, this relation allows the determination of the onset potential of oxide formation in the electrolyte from an extrapolation to a vanishing breakdown potential. This is equal to a film thickness of 0 nm. This potential is determined to be $\sim$1.6 V (HESS) for aluminium. This value is in good agreement with that one found by Takahashi et al. [19].

It should be pointed out clearly, that no assumptions or prerequisites are necessary for this determination. Other methods such as charge over potential plot, reciprocal capacity over potential plot, sputter depth profiling and ellipsometry generally need plausible parameters such as mole volume, dielectric constant or film formation factor.

In the plot presented here no such things are necessary, since from the breakdown potential vs. formation potential plot only a relative shift is determined for a unity slope.

The calculation of the film thickness of course have to make assumptions. As already discussed in a previous work a value of 1.6 nm V^{-1} is used for Al [10]. This value is the key parameter of a consistent set of physical parameters determined from different methods (impedance spectroscopy, current transients of potentiostatic pulse experiments, ellipsometry, XPS). The slope of the line gives directly the breakdown field strength.

$$\frac{dU_{BD}}{dd} = E_{BD} \tag{12}$$

This breakdown fieldstrength has a value of 625 MV m^{-1} for aluminium. It should be mentioned here, that this finding of a constant breakdown field strength was already reported by De Wit et al. [20,21]. Their results were in clear contrast to those of other authors (cited in [20,21]), which found a decreasing breakdown fieldstrength with increasing film thickness. The experiments of De Wit et al. were performed on thicker aluminium films (23–169 nm).

For oxide types as gas phase oxidation or physical vapour deposition the mean variation of the breakdown potential is significantly strong. For physical vapour deposited specimen a clear relationship between breakdown voltage and film thickness cannot be observed. Several samples with 10 or 15 nm thick oxide films were investigated, their breakdown voltages vary in a wide range of 1.7 V until 3.2 V for both oxide thicknesses. These values are shown as bars in Fig. 4. This may be due to the porous and thereby hardly reproducible structure of this oxide type. Thereby in the following the focus is set on anodic oxides on various base metals.

The same set of experiments as in Fig. 4 was carried out for the following valve metals: Hafnium, Niobium, Tantalum, Titanium and Zirconium. During the anodic oxide formation the film formation factor of each metal was determined from a set of subsequent experiments, where coulometric and capacitance measurements were performed. If the oxide formation charge is plotted as a function of the film formation potential, the slope gives the so-called film formation factor k (Eq. (3)). For a potentiostatic oxide formation procedure, there is an reciprocal correlation between the film formation factor k and the formation field strength E_{form}:

$$E_{form} \equiv \frac{1}{k} \tag{13}$$

In Fig. 5 the breakdown fieldstrength for all valve metals investigated in this study is plotted vs. the formation fieldstrength. The straight line does not show a regression of these data points but the function where breakdown fieldstrength and formation fieldstrength are equal. There is an inherent coincidence of both values. This means that the process being responsible for these phenomena is the same in both cases. In the upper x-axis the film formation factor k of the anodic oxide formation is given.

The strong correlation between breakdown fieldstrength and film formation field strength suggests a common origin. As already discussed above, the number of mobile ions increases significantly during oxide formation. If a valve metal which is covered by an anodic oxide film is polarised to a certain potential the current becomes stable after some time. In Fig. 1 this is the case for times longer than 100 s, but this time depends very much on the exact anodising conditions. However, under steady state corrosion conditions the defect concentration is constant. Under the preparation conditions used here, where the sample is removed from the electrolyte under potentiostatic conditions these defects are frozen in. Also Azumi and Ohtsuka [22] proposed the presence of high valence states such as Ti^{5+} or Ti^{6+} in thin anodic oxide films on titanium. Later, after evaporation of the silver cover electrode when the breakdown is observed in the MIM configuration, the same concentration of defects with the same energetic distribution is still present. Those defects which where mobile at lower energies had been already removed under the steady state corrosion conditions. Hence, there is a threshold energy above which defects are existent in the oxide. As a result no breakdown is observed for potentials below this level, since no defects can be mobilised. The experimental results thereby prove that no additional defects are produced through the evaporation procedure.

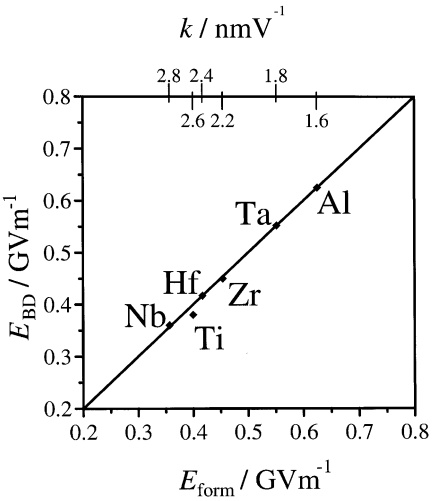

Fig. 5. Breakdown fieldstrength E_{BD} at $T=298$ K for different valve metals as a function of the respective formation fieldstrength E_{form}. The respective formation factor is given in the upper abscissa for comparison. The full line shows where breakdown fieldstrength and formation fieldstrength are identical.

In Fig. 6 a current transient of a complete breakdown process of an aluminium oxide layer in MIM configuration at room temperature is shown. The time to breakdown is indicated by an arrow. For times up to 30 μs the transient is dominated by the Debye charging of the oxide capacitance. The time constant of this charging depends on the capacity and on the contact resistance. Later the transient is dominated by the tunnel current. This is indicated by the parallel resistance R_i in the simple equivalent circuit. The correlation between parts

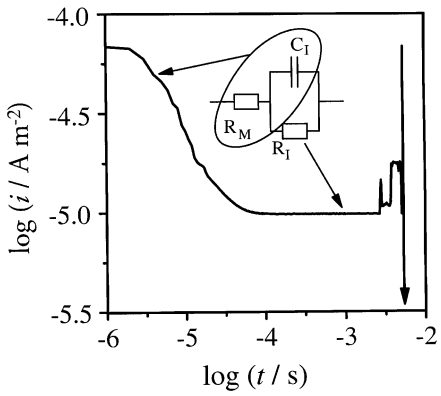

Fig. 6. Current transient of a complete breakdown process. The time to breakdown is indicated by an arrow. R_I, C_I, mean the resistivity and the capacity of the insulator. R_M means the contact resistivity of the metal. The correlation between parts of the simple equivalent circuit diagram and the different parts of the transient is also indicated.

of the simple equivalent circuit diagram and the different parts of the transient is also indicated.

The tunnel current is very constant up to a few milliseconds. After a few ms a sudden increase is observed. The current stabilises then for a short time on slightly higher level. Then a second sudden increase occurs and the current stabilises on level B which is again higher than before. Finally, a few short fluctuations in the current density indicate the final breakdown during which the current increases to the short circuit level. This high current causes an irreversible damage of the electrical connector which burns down like a fuse. Remarkably the step like increase of the tunnel current when a voltage greater than the film formation potential was applied could be found in all of our samples. The duration of period A and B varied about a range of several 100% for this experiment. But they appeared always as a kind of precursor of the anodic breakdown.

5. Discussion

The common collision ionisation model of the electric breakdown as summarised by O'Dwyer [23] requires a sufficiently high probability for the ionisation process. For the very thin oxide films ($d=2.5-15$ nm) investigated here single electron tunnel processes are significantly more probable than interaction processes such as collision ionisation. Thereby the experimental results are discussed in terms of ionically distorted tunnel barriers.

If the fieldstrength in the MIM contact exceeds the former film formation fieldstrength some defects with the critical activation energy become mobile. The movement of these defects will then initiate the breakdown by means of enhanced electronic tunnelling. A distortion of tunnel barriers due to ionic defects in the insulator was already discussed by Schmidlin et al. [24]. In their calculations they derived significant tunnel current increases due to the barrier deformation caused by ionic defects.

On the other hand, a defect which is only slightly shifted within the oxide can modify the tunnel path of the electrons and serve as a centre for resonance tunnelling. Due to the shortening of the effective tunnel length the current will increase significantly. This current may locally heat the sample adjacent to the tunnelling path. This heating at a given fieldstrength on the other hand will activate further defects. An additional barrier deformation will result, which will cause a further increase in the tunnel current. Within this positive feedback loop various processes like sample heating, increasing current flow and mobilisation of ionic defects may contribute to the final breakdown.

In fact this activation of defects is more complex. The process does not only depend on the potential but also on the temperature and the time for which the sample is polarised. Current transients of potentiostatic pulse steps with voltages above the critical breakdown value show a significant transient behaviour. The destructive processes occur after times which can be easily resolved in the experiments presented here (see Fig. 6). For short times ($t<1$ ms) a sample can survive above its breakdown fieldstrength.

Further experiments show that the breakdown is significantly shifted to higher potentials and longer times at lower temperatures ($T<100$ K). These experiments and a toughening procedure derived therefrom will be described in the next part of this work.

6. Conclusion

The breakdown of MIM contacts with various oxide types and thicknesses in the range 2–15 nm was studied. While GPO and PVD oxides showed a large mean deviation of the breakdown voltage for a given thickness, anodic oxides showed a highly reproducible and predictable breakdown voltage. In the breakdown voltage vs. formation potential plot an excellent linearity with the unity slope is achieved for the anodic oxide systems. The absolute deviation from this line was always smaller than 50 mV.

An extrapolation of the obtained line down to zero breakdown voltage gives the film formation potential of the anodic oxide formation in the corresponding electrolyte. It has a value of -1.6 V (HESS) which coincides with the thermodynamic value [25]. If the breakdown voltage is plotted vs. film thickness as calculated from the charge consumed during oxide formation, the slope gives the breakdown fieldstrength of the oxide.

The reciprocal of the film formation factor gives directly the film formation fieldstrength. It turns out that, both film formation fieldstrength and breakdown fieldstrength are almost identical. This coincidence was

shown for aluminium, hafnium, niobium, tantalum, titanium and zirconium.

Acknowledgments

The financial support of the Deutsche Forschungsgemeinschaft is gratefully acknowledged. The authors wish to thank M.M. Lohrengel for helpful discussions.

References

[1] C.J. Kaiser, Capacitor Handbook, C.J. Publishing, 1995.
[2] J. Drucker, K. Hansma, Phys. Rev. B 30 (1986) 4348.
[3] G. Mende, F. Fenske, H. Flietner, M. Jeske, J.W. Schultze, Electrochim. Acta 39 (1994) 1259.
[4] V.K. Agarwal, Thin Solid Films 24 (1974) 55.
[5] P. Solomon, J. Vac. Sci. Technol. 14 (1977) 1122.
[6] N. Klein, in: L. Marton (Ed.), Advances in Electronics and Electron Physics, vol. 26, Academic Press, New York, 1969.
[7] T.H. DiStefano, M. Schatzkes, J. Vac. Sci. Technol. 13 (1976) 50.
[8] S. Ikonopisov, Electrochim. Acta 22 (1977) 1077.
[9] V. Parkhutik, J.M. Albella, J.M. Martinez Duart, in: B.E. Conway (Ed.), Modern Aspects of Electrochemistry, No. 23, Plenum Press, New York, 1992, p. 315ff.
[10] D. Diesing, A.W. Hassel, M.M. Lohrengel, Thin Solid Films 342 (1999) 282.
[11] A.M. Shousha, J. Non-Cryst. Solids 17 (1975) 100.
[12] M.M. Lohrengel, Mater. Sci. Eng. R 11 (1993) 243.
[13] C.B. Duke, Tunneling in Solids, Academic Press, New York, 1969, p. 62.
[14] J.G. Simmons, J. Appl. Phys. 35 (1964) 2655.
[15] J.G. Simmons, J. Appl. Phys. 34 (1963) 1793.
[16] D. Diesing, Thesis, Heinrich-Heine-Universität Düsseldorf (1996).
[17] A.W. Hassel, Thesis, Heinrich-Heine-Universität Düsseldorf (1997), Verlag Shaker, Aachen (ISBN 3-8265-2981-2).
[18] A. Haque, A.N. Khondker, Phys. Rev. B 52 (1995) 11193.
[19] H. Takahashi, K. Fujiwara, M. Seo, Corros. Sci. 36 (1994) 689.
[20] H.J. De Wit, C. Crevecoeur, Phys. Lett. 50 (1974) 365.
[21] H.J. De Wit, C. Wijenberg, C. Crevecoeur, J. Electrochem. Soc. 123 (1976) 1479.
[22] K. Azumi, T. Ohtsuka, Zairyo to Kankyo 46 (1997) 384.
[23] J.J. O'Dwyer, The Theory of Electrical Conduction and Breakdown in Solid Dielectrics, Clarendon Press, Oxford, 1973.
[24] F.W. Schmidlin, J. Appl. Phys. 37 (1966) 2823.
[25] M. Pourbaix, Atlas of Electrochemical Equilibria in Aqueous Solutions, Cebelcor, Brussels (1974), p. 168.